Mon. Not. R. Astron. Soc. **000**, 000–000 (0000) Printed 18 October 2012 (MN LaTeX style file v2.2)

arXiv:1210.4750v1 [astro-ph.GA] 17 Oct 2012

On the possibility of a warped disc origin of the inclined stellar discs at the Galactic Centre

A. Ulubay-Siddiki[1⋆], H. Bartko[2], and O. Gerhard[2]
[1] *Istanbul University, Faculty of Science, Department of Physics, 34134 Vezneciler, Istanbul, Turkey*
[2] *Max-Planck-Institut für Extraterrestrische Physik,Giessenbachstraße, D-85748 Garching, Germany*

18 October 2012

ABSTRACT

The central parsec of our Galaxy hosts a population of young stars. At distances of $r \sim 0.03$ to 0.5 pc, most of these stars seem to form a system of mutually inclined discs of clockwise and counter clockwise rotating stars. We present a possible warped disc origin scenario for these stars assuming that an initially flat accretion disc becomes warped due to a central radiation source via the Pringle instability, or due to a spinning black hole via the Bardeen-Petterson effect, before it cools, fragments, and forms stars. From simple arguments we show that this is plausible if the star formation efficiency is high, $\epsilon_{\rm SF} \lesssim 1$, and the viscosity parameter $\alpha \sim 0.1$. After fragmentation, we model the disc as a collection of concentric, circular rings tilted with respect to each other, and construct time evolution models of warped discs for mass ratios and other parameters relevant to the Galactic Centre environment, but for also more massive discs. We take into account the disc's self-gravity in the non-linear regime and the torques exerted by a slightly flattened surrounding star cluster. Our simulations show that a self-gravitating low-mass disc ($M_{\rm d}/M_{\rm bh} \sim 0.001$) precesses with its integrity maintained in the life-time of the stars, but precesses essentially freely when the torques from a non-spherical cluster are included. An intermediate-mass disc ($M_{\rm d}/M_{\rm bh} \sim 0.01$) breaks into pieces which precess as independent discs in the self-gravity-only case, and become disrupted in the presence of the star cluster torques. Finally, for a high mass disc ($M_{\rm d}/M_{\rm bh} \sim 0.1$) the evolution is dominated by self-gravity and the disc is broken but not dissolved. The time-scale after which the disc breaks into pieces scales almost linearly with $M_{\rm d}/M_{\rm bh}$ for self-gravitating models. Typical values are longer than the age of the stars for $M_{\rm d}/M_{\rm bh} \sim 0.001$, and are in the range $\sim 8 \times 10^4 - 10^5$ yr for $M_{\rm d}/M_{\rm bh} \sim 0.1 - 0.01$ respectively. None of these discs explain the two Galactic Centre discs with their rotation properties. A comparison of the models with the better-defined clockwise rotating disc shows that the lowest mass model in a spherical star cluster matches the data best.

1 INTRODUCTION

The centre of our Galaxy hosts a supermassive black hole (SMBH), SgrA*, with a mass of $3.95 \pm 0.06 \times 10^6\ M_\odot$ (Genzel et al. 2000; Ghez et al. 2005; Trippe et al. 2008; Gillessen et al. 2009). SgrA* is surrounded by a cluster of old (Trippe et al. 2008; Schödel et al. 2009), as well as a group of young stars (Krabbe et al. 1995; Genzel et al. 2003; Levin & Beloborodov 2003; Paumard et al. 2006; Lu et al. 2006, 2009; Bartko et al. 2009, 2010).

Of the 136 young stars observed at distances ~ 0.05 pc to ~ 0.5 pc, 59 populate a disc (Genzel et al. 2003; Levin & Beloborodov 2003; Paumard et al. 2006; Lu et al. 2006, 2009; Bartko et al. 2010) which is observed to rotate clockwise (CW) on the plane of sky. Of the rest, 20 stars seem to populate an other disc highly inclined to the CW one (Genzel et al. 2003; Paumard et al. 2006; Bartko et al. 2009, 2010), and rotating counter clockwise (CCW) on the sky (but also see Lu et al. (2006)). Ages of these young stars are consistent with being a few Myr, suggesting that there has been a star formation episode in the Galactic Centre (GC) a few million years ago.

In order for a molecular cloud near a SMBH to fragment into stars, its self-gravity should overcome the tidal field of the black hole. This requirement for star formation poses a constraint on the minimum cloud densities, which are orders of magnitude higher than the observed cloud densities near the GC. However theoretical estimates suggest that the fragmentation conditions are met naturally on the accretion discs which become self-gravitating beyond a few tenth of parsec (Kolykhalov & Syunyaev 1980; Gammie 2001; Goodman 2003). Therefore, several numerical simulations have been performed aiming at modeling the in-situ fragmentation of a nuclear/accretion disc for parameters relevant to the GC. The simulations were run either assuming *a priori* gravitationally unstable accretion disc already in place (Nayakshin et al. 2006; Alexander et al. 2008), or trying to account also for the formation of the disc itself through infall of molecular clouds into the vicinity of the black hole (Bonnell & Rice 2008; Mapelli et al. 2008; Hobbs & Nayakshin 2009).

Today it looks like a star forming disc at the GC can be simulated, albeit perhaps for a somewhat fine-tuned parameter range. On the other hand, apart from the problem of youth, another issue still to be addressed is the distribution of the inclinations of the stars. It is reasonable to expect that a planar accretion disc leaves behind a planar distribution of stars when it fragments, but the recent data published by Bartko et al. (2009) provide evidence for a warp in the CW disc with an amplitude of about 60°. Lu et al. (2009) point out that even though the stars might have formed in-situ, their current orbital distribution suggests a more sophisticated origin than a simple thin accretion disc. Simulations performed by Cuadra et al. (2008) are in line with this idea showing that once the stars form on a cold accretion disc it is not possible to perturb these stars to the high inclinations at which they are observed. Kocsis & Tremaine (2011) showed that vector resonant relaxation between the disc and the surrounding old star cluster might excite a warp in the disc if the stochastic torques from the star cluster dominate over the disc's self-gravity. Recently, Haas et al. (2010) considered the evolution of the stellar disc using N-body simulations. Their simulations successfully produced the relative inclination between the stellar disc and the surrounding Circumnuclear Disc, however the origin of the disc was not addressed.

Warped discs, although monitored only through maser emission from gas discs, exist on similar scales in other nearby galactic nuclei such as NGC4258 (Herrnstein et al. 1996), NGC1068 (Greenhill & Gwinn 1997), and Circinus (Greenhill et al. 2003). An initially planar accretion disc could become warped when torqued by a spinning black hole (Bardeen & Petterson 1975; Armitage & Natarajan 1999; Lodato & Pringle 2007; Martin 2008), when exposed to radiation from a central source (Petterson 1977; Pringle 1996, 1997), or when subject to the torques induced by the stars in a stellar cusp around the black hole (Bregman & Alexander 2009). Milosavljević & Loeb (2004) pointed out that the maser nuclei, and the Galactic Centre might represent different epochs of a cycle during the lifetime of a typical spiral galaxy.

In this paper, we investigate alternative scenarios for the formation of a star-forming, warped disc at the Galactic Centre. Accordingly, a flat accretion disc forms around SgrA*, extending out to the location of the young stars observed today. During a supposed period of active accretion, the disc is illuminated by the central source, or torqued by a spinning black hole, and becomes warped due to the Pringle instability or the Bardeen-Petterson effect, respectively. When the AGN activity subsides, the disc cools and forms stars. Afterwards, the stellar disc evolves in the gravitational field of the black hole, its own self-gravity, and the surrounding old star cluster. We investigate under which conditions this scenario could work, and show that with a low mass such as inferred today the remnant warped stellar disc largely survives for the life-time of the observed young stars.

In §2 we work out the conditions for which the disc would become warped due to the mechanisms mentioned above, and then fragment into stars. In §3 we describe our model and the numerical scheme for studying the subsequent time evolution of the warped stellar disc. The results of our simulations are presented in §4 where a comparison with the observations is also made. In §5 we present a discussion, and in §6 we summarize our results, and our conclusions.

2 WARPING THE GALACTIC CENTRE DISC

In this section, we discuss a plausible scenario of how a disc of young stars in the Galactic Centre might have acquired its warped shape. We start with the assumption that an accretion disc builds up, leading to an active phase of sub-Eddington accretion onto the Galactic Centre black hole. We then investigate two possible mechanisms: radiation pressure instability (Petterson 1977; Pringle 1996, 1997) and Bardeen-Petterson effect (Bardeen & Petterson 1975) for warping the accretion disc, which have both been extensively discussed in the context of the maser discs in nearby Seyfert galaxies (Maloney et al. 1996; Scheuer & Feiler 1996; Pringle 1997; Armitage & Natarajan 1999; Lodato & Pringle 2007; Martin 2008).

We further assume that after some time the accretion and energy production is reduced, which is followed by a period where the warped disc can cool and form stars. Thereafter the stellar disc is only subject to gravity, precessing under the influence of the gravitational torques from the disc itself, and the surrounding old star cluster.

In §2.1, we constrain the surface density of the disc prior to fragmentation from the observed number density of young stars. In the following subsections 2.2 and 2.3, we consider in turn warping by the radiation pressure instability and the Bardeen-Petterson effect. In §2.4, we compare the radiation, viscous, and gravitational torques on the disc, and in §2.5 we consider fragmentation and star formation.

2.1 Surface Density of the Disc Prior to Fragmentation

The warping mechanisms which we will briefly consider in sections (2.2) and (2.3) are generally studied within the framework of viscous, steady-state accretion discs. As such they make use of a number of parameters which from the observations of the stellar discs can not be tested or constrained. For these, we will mostly refer to the canonical values for AGN discs when needed. Still, there is one parameter, the surface density of the supposed gaseous disc which may be determined by the observations. To do so we make use of the stellar number counts on the GC discs. The total number of stars $N_\star$ in a stellar population can be calculated by writing

$$N_\star = \int_{M1}^{M2} \xi(M) dM, \tag{1}$$

where $\xi(M)$ is the initial mass function, IMF, and M_1 and M_2 are the lowest and highest stellar masses assumed to exist in this population. The IMF describes how the mass is distributed in stars in a newly born population. For a given

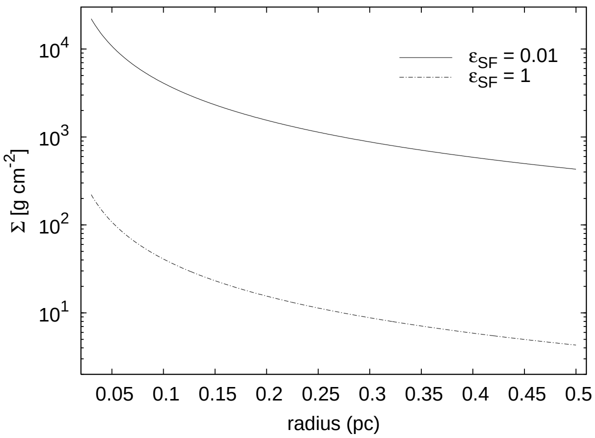

Figure 1. Surface density of the supposed GC gaseous disc for star formation efficiencies of 0.01 (solid line), and 1 (dotted line).

IMF, the total mass in stars, M_s, is calculated from

$$M_{\rm s} = \int_{M1}^{M2} M\xi(M)dM. \tag{2}$$

Bartko et al. (2010) deduce an IMF of $\xi(M) = \xi_0 M^{-0.45}$ for the GC discs. The Bartko et al. (2010) sample includes 59 stars in the CW disc, and 20 stars in the CCW disc. Using equations (1) and (2), and assuming a lower mass end of $1M_\odot$, and an upper mass end of $120M_\odot$, the current total stellar mass in the discs can be found to be $M_{\rm s}|_{\rm CW} + M_{\rm s}|_{\rm CCW} = M_{\rm s} \sim 5360M_\odot$, where $M_{\rm s}|_{\rm CW}$, and $M_{\rm s}|_{\rm CCW}$ are the masses of the CW and CCW rotating discs respectively. The mass of the Galactic central black hole is $\sim 4\times 10^6 M_\odot$, so the inferred disc mass corresponds to a mass ratio $M_{\rm d}/M_{\rm bh} = 0.00134$.

The total stellar disc mass inferred today is a fraction of the mass of the original gaseous disc since presumably not all the gas was converted to stars. Assuming a star formation efficiency $\epsilon_{\rm SF}$ the total mass of the seed disc can be calculated. Since the radial extent of the discs is observationally constrained, this mass can be converted into a surface density Σ of the proposed gas disc. The observations of the stellar discs suggest that the mass density decreases nearly as $1/r^{1.4}$ (Bartko et al. 2010), so we write for the mass $M_{\rm d}$ of the gaseous disc

$$M_{\rm d} = 5360\mu_{5360}\epsilon_{\rm SF}^{-1}M_\odot, \tag{3}$$

where $\mu_{5360} = (M_{\rm s}/5360M_\odot)$ and for the surface density $\Sigma_{\rm d}(r) = \Sigma_{0.1}\hat{r}^{-1.4}$ we find

$$\Sigma_{0.1} = 9.52\times 10^4 \mu_{5360}\epsilon_{\rm SF}^{-1}\frac{\rm M_\odot}{\rm pc^2} = 19.89\mu_{5360}\epsilon_{\rm SF}^{-1}\frac{\rm g}{\rm cm^2}, \tag{4}$$

with $\hat{r} \equiv r/0.1$pc. In Fig. 1 we show for two star formation efficiencies the surface density of the disc obtained as described above. The solid line assumes $\epsilon_{\rm SF} = 0.01$, and the dotted line assumes $\epsilon_{\rm SF} = 1$.

2.2 Radiation Driven Warping and the Galactic Centre Disc

Radiation warping of accretion discs is studied in detail by many authors (Pringle 1996; Maloney et al. 1996; Pringle 1997; Ogilvie & Dubus 2001). When an optically thick disc is exposed to central radiation, and it re-emits the absorbed incident photons parallel to the disc local normal, an inward directed force is experienced by each side of the disc. If the disc is slightly distorted, a net torque is induced which results in a modification of the warp, and precession of the disc around the total angular momentum direction. Whether the disc will acquire a pronounced warp or not depends on the competition between the net torque, and the component of the stress in the $r-z$ direction in cylindrical symmetry, present in warped discs. The latter forces the disc to settle onto a plane on an alignment time-scale. The alignment time scale at distance r from the black hole is associated with the $r-z$ stress, and can be written as $t_{\nu_2} = 2r^2/\nu_2$, where ν_2 is the vertical viscosity coefficient. The condition that the warp growth time scale, t_Γ, be smaller than the viscous time scale, t_{ν_2} is written as (Pringle 1997)

$$\frac{12\pi\Sigma r^3\Omega c}{L} \leqslant \frac{2r^2}{\nu_2}, \tag{5}$$

where L is the luminosity of the central source, c is the speed of light, and α is the Shakura-Sunyaev parameter (Shakura & Sunyaev 1973). Equation (5) assumes an accretion disc which is in steady state. For such discs, the luminosity of the disc L is related to the radiative efficiency $\epsilon \equiv L/\dot{M}c^2$, where $\dot{M}$ is the mass accretion given by $\dot{M} = 3\pi\Sigma\nu_1$, and ν_1 is the radial viscosity coefficient. In order to evaluate the warping criterion given in (5) one has to estimate the magnitude of the vertical viscosity ν_2. Previous studies of linear hydrodynamic warps and magnetized shearing box simulations of accretion discs showed that $\eta_\nu = \nu_2/\nu_1 = 1/2\alpha^2$ (Papaloizou & Pringle 1983; Ogilvie 1999; Torkelsson et al. 2000). Lodato & Pringle (2007) find with smoothed particle hydrodynamics simulations of small and large-amplitude warps that the vertical viscosity saturates for small α such that $\eta_\nu < 3.5/\alpha$. Using these, the warp damping time scale becomes

$$t_{\nu_2} = \frac{2r^2}{\nu_2} \simeq \left(\frac{\alpha}{3.5}\right)\frac{2r^2}{\nu_1} \approx 5.6\times 10^5 \frac{\alpha\mu_{5360}\epsilon\hat{r}^{0.6}}{\epsilon_{\rm SF}\eta_{\rm edd}}{\rm yr}, \tag{6}$$

where $\eta_{\rm edd} \equiv L/L_{\rm edd}$. Equation (5) can now be rearranged to give the radiation warping critical radius

$$R_{\rm rad} > \frac{2\eta_\nu^2}{\gamma_{\rm crit}^2\epsilon^2}\frac{2GM_{\rm bh}}{c^2}, \tag{7}$$

where $\gamma_{\rm crit} \simeq 0.32$ (Pringle 1997). One way to obtain a stronger torque is if the irradiation of the disc is driving an outflow (Schandl & Meyer 1994). In this case, the torque is determined by the outflow momentum or pressure at the sonic point, which is basically $\propto L$, but also depends on the detailed disc structure in a complicated way. The enhancement of the torque could be significant, as the ratio of momentum to energy for particles may be much larger than for photons. Although a gross over simplification, we may parameterize this by an additional (not constant) multiplicative factor $F_{\rm wind}$ on the radiation torque, so that the warping criterion becomes

$$R_{\rm rad} > \frac{2\eta_\nu^2}{\gamma_{\rm crit}^2\epsilon^2F_{\rm wind}^2}\frac{2GM_{\rm bh}}{c^2} = 9.1\times 10^{-3}\alpha^{-2}\epsilon_{0.1}^{-2}F_{\rm wind}^{-2}\ {\rm pc}, \tag{8}$$

where for the numerical value we have used $\gamma_{\rm crit} \simeq 0.32$, $\epsilon = 0.1\epsilon_{0.1}$ and $\eta_\nu \simeq 3.5/\alpha$. Thus warping the disc in the radial range of the GC discs (0.03-0.5pc) requires $\alpha \sim 0.3$, or $\alpha \sim 0.1$ and radiatively efficient accretion by a rotating black hole or modest enhancement of the torque by a disc wind.

2.2.1 The Effect of Warping on Irradiation and Fragmentation

Having argued for the possibility of radiation warping of the past accretion disc at the GC, we now discuss the feedback effect of warping on the irradiation and fragmentation of the disc.

Pringle (1997) studied the growth and non-linear evolution of radiation induced warps in the context of AGN accretion discs. His simulations show that highly warped discs exhibit limit cycle oscillations as a consequence of self-shadowing. As the warp gradually grows, the solid angle subtended by the central source decreases. When the maximum inclination of π is reached, the instability cuts off leading to a decrease of the disc inclination. Thereafter, the disc geometry again lets the instability set in, and the warp grows. Hence, even though the disc might be warped by large angles, radiation instability keeps acting on the disc so long as there is sufficient amount of radiation from the central parts.

The effect of warping on fragmentation is studied in Goodman (2003) who estimated for an irradiated disc the stabilizing temperature, $T_{\rm st}$, above which fragmentation can not occur. When $T_{\rm st}$ is much larger than the temperature of the disc in equilibrium with radiation from the central source $T_{\rm eq}$, irradiation can not prevent fragmentation even for highly warped discs. The ratio $T_{\rm st}/T_{\rm eq}$ depends (weakly) on the mass of the central object and for a black hole of mass $M_{\rm bh} = 4 \times 10^6 M_\odot$, and a disc with a warp of 60° it becomes ~ 1 at 0.03 pc and ~ 4 at 0.5 pc for $\alpha = 0.3$, and $\epsilon = 0.1$. We note that for a disc around a black hole of mass $M_{\rm bh} = 10^8 M_\odot$, this ratio would have a value > 10 at all radii, therefore fragmentation for a surrounding disc would be most likely. For the case of the GC on the other hand, the ratio $T_{\rm st}/T_{\rm eq}$ being close to unity at the inner edge of the disc suggests that fragmentation might be somewhat delayed until the effect of irradiation on the disc diminishes (see §2.5).

2.3 Bardeen Petterson Effect and the Galactic Centre Stellar Disc

In this section, we show under which conditions the Galactic Centre disc might have been warped due to Bardeen-Petterson effect.

An accretion disc forming around a rotating (Kerr) black hole might initially have a total angular momentum misaligned with that of the black hole. Inner portions of the disc close to the black hole experience general relativistic frame dragging which causes a differential precession, the so-called Lense-Thirring precession (Lense & Thirring 1918). As we have seen in the previous section, the viscous time scale increases with radius, hence the inner parts of the disc are forced to align with the black hole on time scales much shorter than those for the outer parts. Consequently, the disc develops a shape which for $r < R_{\rm BP}$ is aligned with the black hole, i.e. is flat, and for $r \geqslant R_{\rm BP}$ its angular momentum direction changes gradually from radius to radius (Bardeen & Petterson 1975). Like the radiation pressure warping, the Bardeen-Petterson effect also is a competition between the alignment time scale, and the precession time scale (Armitage & Natarajan 1999). The precession induced by the Bardeen-Petterson effect is given by (Kumar & Pringle 1985)

$$\dot{\phi} = 2ac\left(\frac{GM_{\rm bh}}{c^2}\right)^2 \frac{1}{r^3}, \qquad (9)$$

where a is the black hole spin parameter which can take values between 0 and 1 for stationary, and maximally rotating black holes respectively. The precession time scale $\tau_{\rm BP} = 2\pi/\dot{\phi}$ is

$$\tau_{\rm BP} = \frac{\pi c^3 r^3}{aG^2 M_{\rm bh}^2}. \qquad (10)$$

The critical radius, where the alignment time scale equals the precession time scale is then obtained by writing

$$\frac{\pi r^3 c^3}{aG^2 M_{\rm bh}^2} = \frac{2r^2}{\nu_2} \rightarrow R_{\rm BP} = \frac{2aG^2 M_{\rm bh}^2}{\pi c^3 \nu_2}. \qquad (11)$$

Using the steady state relations introduced in the previous section equation (11) becomes

$$R_{\rm BP} = \frac{6aG^2 M_{\rm bh}^2 \epsilon \Sigma(R_{\rm BP})}{\eta_\nu c L}. \qquad (12)$$

In order to estimate the Bardeen-Petterson radius for the GC, we need to solve equation (12) for $R_{\rm BP}$. Writing $\Sigma(R_{\rm BP}) = \Sigma_0/\hat{r}^{-1.4}$ we obtain

$$R_{\rm BP} = 4.22 \times 10^{-4} \left(\frac{a\epsilon\alpha\mu_{5360}}{\eta_{\rm edd}\epsilon_{\rm SF}}\right)^{1/2.4} \ {\rm pc}. \qquad (13)$$

This estimate shows that the Bardeen-Petterson radius for the GC is quite small, i.e. much below the inner edge of the observed discs. We should remind that the alignment time scale t_{ν_2} for the assumed surface density profile is short. This means that the disc can be warped out to large distances since both $R_{\rm BP}$ and t_{ν_2} depend on the disc parameters only weakly.

The angular momentum of the disc at r is $\propto 2\pi\Sigma r dr\sqrt{GM_{\rm bh}r} \propto r^{0.1}dr$ and varies only slowly with r. The ratio of the disc to black hole angular momenta can thus be estimated as

$$\frac{J_d}{J_{\rm bh}} \simeq \frac{M_d\sqrt{GM_{\rm bh}r_d}}{aGM_{\rm bh}^2/c} = \frac{1}{a}\frac{M_d}{M_{\rm bh}}\sqrt{\frac{2r_d}{r_s}} \sim 0.97\epsilon_{\rm SF}^{-1}a^{-1}, \qquad (14)$$

where $r_{\rm s} = 2GM_{\rm bh}/c^2$ is the Schwarzschild radius, and $r_{\rm d} \sim 0.1$ pc. This suggests that by the time the disc is significantly warped at $r_{\rm d} \sim 0.1$ pc, the black hole spin should be significantly aligned: the alignment time-scale found by Lodato & Pringle (2006) under similar circumstances is $\sim 0.3t_{\nu_1} \sim 0.3(3.5/\alpha)t_{\nu_2} \sim \alpha^{-1}t_{\nu_2}$. These arguments suggest that if the GC disc was first warped through the Bardeen-Petterson effect, and then fragmented to form the observed surface density of young stars, the star formation efficiency had to be high, $\epsilon_{\rm SF} < 1$, to prevent the disc from dominating the angular momentum, and $\alpha < 0.1$ to give the disc time to warp before it is accreted and will align the black hole spin.

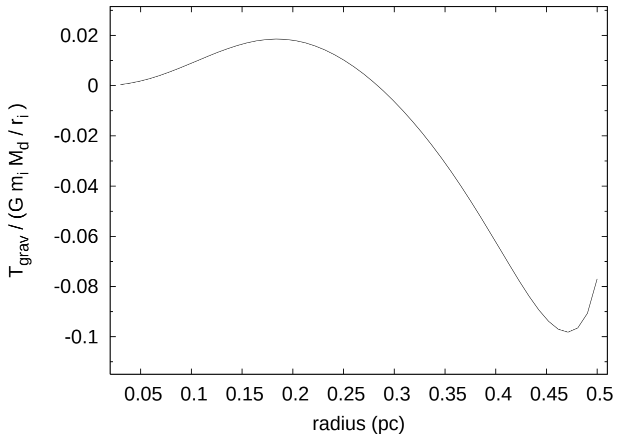

Figure 2. Normalized gravitational torque for the GC disc when the warp spans a range of $-15°\to 15°$ in inclination.

2.4 Comparison of Gravitational, Viscous and Radiation Torques

In §2.2 we have discussed the conditions for radiation warping. While equation (5) has to be satisfied for warping, it is also useful to compare the magnitude of radiation and gravitational torques acting on the disc.

The magnitude of the radiation torque on a ring of radius r with radial width dr can be approximated as (Ogilvie & Dubus 2001)

$$2\pi r dr T_\Gamma \simeq \frac{L}{6cr} r dr, \tag{15}$$

thus $T_\Gamma = \Sigma r^2\Omega/t_\Gamma$. On the other hand the viscous torque on the ring, which tries to damp the warp in the case of radiation pressure warping, and which sets up the warped density distribution in the Bardeen-Petterson mechanism, is given by

$$2\pi r dr T_{\nu_2} = \frac{\Sigma r^2 \Omega 2\pi r dr}{2r^2/\nu_2} = \frac{\eta_\nu L \Omega r dr}{3\epsilon c^2}. \tag{16}$$

The gravitational torque of the disc on the same ring can be determined by integrating over the disc

$$2\pi r dr T_{\rm grav} \simeq \frac{G M_d \Sigma(r) 2\pi r dr}{r} J, \tag{17}$$

where $J \equiv T_{\rm grav}/(G m_i M_d/r_i)$ is a dimensionless integral depending on r/r_1, r/r_2

$$J = \int_{r_1}^{r_2} \frac{2\pi r' dr' \Sigma(r')}{M_d} \frac{r^2 r'}{(r'^2+r^2)^{3/2}} \sin(2\beta)\, I(\beta, r/r') \frac{\partial\beta}{\partial\theta}, \tag{18}$$

and where $\beta(r,r')$ is the angle between the normals of the two rings at r and r', θ is the inclination of the ring at r, so $\partial\beta/\partial\theta = O(1)$, and $I(\beta, r/r')$ is the integral in equation (13a) of Ulubay-Siddiki et al. (2009) (hereafter US09).

We show in Fig. 2 the values of the J-terms at different distances from the black hole when the warp spans a range of $-15° \to 15°$ in inclination. For larger warps, the gravitational torques are weaker. Also if we include the part of the disc outside $[r_{\rm in}, r_{\rm out}]$ the product $M_{\rm d} J$ decreases as the torques are dominated by the nearby parts of the disc. Using the surface density profile above, the ratio of the radiation and gravity torques is

$$\frac{T_\Gamma}{T_{\rm grav}} = \frac{L}{6cr}\frac{r}{2\pi G M_{\rm d}\Sigma(r) J} = 32.5 \frac{\eta_{\rm edd}\epsilon_{\rm SF}^2}{\mu_{5360}^2}\frac{\hat{r}^{1.4}}{J}, \tag{19}$$

and the ratio of the viscous torque to the gravitational torque is

$$\frac{T_{\nu_2}}{T_{\rm grav}} = \frac{\eta_\nu L \Omega}{3\epsilon c^2}\frac{r}{2\pi G M_{\rm d}\Sigma(r) J} = 3.14 \frac{\eta_{\rm edd}\epsilon_{\rm SF}^2}{\mu_{5360}^2 \alpha \epsilon_{0.1}}\frac{\hat{r}^{0.9}}{J}. \tag{20}$$

We see from Fig. 2 that the J-terms for the Galactic Centre disc surface density profile are typically $O(0.1)$. Thus at $r = 0.1$ pc $T_\Gamma \gg T_{\rm grav}$ if $\epsilon_{\rm SF} < 1$, but not if $\epsilon_{\rm SF} \ll 1$. For a high central luminosity $\eta_{\rm edd}$ and/or high star formation efficiency $\epsilon_{\rm SF}$ the viscous torque on the disc dominates over its self-gravity. We have also seen for the case of the Bardeen-Petterson effect that $\epsilon_{\rm SF} < 1$. This shows that it is justified to neglect the effects of the gravitational torques on the evolution of the disc in its active phase.

2.5 The Warped Stellar Disc After Fragmentation

In sections (2.2) and (2.3) we have seen that for a range of assumed accretion disc parameters, the disc at the GC could have been warped in the accretion phase. The evolution of the disc is likely to be governed by the viscous or radiation torques during this phase.

We now assume that some time after the disc has become warped, the active phase of the GC ends. Since $\eta_{\rm edd}$ and the accretion rate will then be highly reduced the disc will receive much smaller energy input and it is reasonable to assume that it can now cool rapidly. If the cooling time is short, fragmentation and star formation can occur on a dynamical time scale (Gammie 2001). The gas content of the disc could then be converted into stars with efficiency $\epsilon_{\rm SF}$ and the rest of the gas will be lost.

Subsequently, the now stellar disc would be subject only to gravitational forces, and precess accordingly. In addition to the precession caused by the disc's self-gravity, the surrounding old star cluster will also contribute unless it is spherically symmetric. After analyzing the proper motions of the old cluster stars, Trippe et al. (2008) reported a small amount of rotation in the direction parallel to the Galactic rotation. The rotation of the old cluster is also confirmed by Schödel et al. (2009). Based on these findings, one might consider the possibility of the star cluster being slightly flattened, hence have an effect on the long term evolution of the disc.

3 WARP MODEL FOR THE GALACTIC CENTRE DISC

In the previous sections we have argued that for a range of parameters, a flat disc around SgrA* could become warped before forming stars, after which the disc evolves gravitationally. In this section, we will introduce the model we have used to follow the time evolution of the warped stellar disc.

3.1 The Equations of Motion

As in US09, we model a warped disc as a collection of concentric circular rings which are tilted with respect to each other. The rings are in gravitational interaction with each other, and are also torqued by the surrounding old star cluster. They are characterized by their masses m_i, and radii r_i. The fast orbital motion around the SMBH of mass $M_{\rm bh}$ is thereby time-averaged. The geometry of the rings is defined by the Euler angles (ψ, θ, ϕ). For a system of n rings, the equations of motion for any of the rings i are given by

$$p_{\theta_i} = \frac{m_i r_i^2}{2}\dot{\theta}_i, \tag{21}$$

$$p_{\phi_i} = \frac{m_i r_i^2}{2}\dot{\phi}_i \sin^2\theta_i + p_{\psi_i}\cos\theta_i, \tag{22}$$

$$\dot{p_{\theta_i}} = \frac{m_i r_i^2}{2}\dot{\phi}_i^2 \sin\theta_i \cos\theta_i - \dot{\phi}_i p_{\psi_i}\sin\theta_i - \frac{\partial V_i}{\partial \theta_i}, \tag{23}$$

$$\dot{p_{\phi_i}} = -\frac{\partial V_i}{\partial \phi_i}. \tag{24}$$

Here $p_{\psi_i} = m_i r_i^2 \Omega_i$ is the orbital angular momentum, $\dot{\phi}_i$ and $\dot{\theta}_i$ are the rates of precession and nutation caused by the torques $\partial V_i/\partial\theta_i$ and $\partial V_i/\partial\phi_i$ respectively, where V_i is the potential energy of ring i in the field of the other rings, and of the old stellar cluster. The details of the calculation of the mutual torques can be found in US09. To calculate the torque due to the surrounding star cluster, we use the description given in Sparke (1986) appropriate for slightly flattened systems. The potential energy of a ring in the field of the cluster is given by

$$V_{\rm cl} = \frac{m_i v_0^2}{6}(1-q)\sin^2\theta_i, \tag{25}$$

where v_0 is the assumed constant circular velocity generated by the star cluster, and q is the flattening. The torque on ring i due to the star cluster is then written as

$$\frac{\partial V_{\rm cl}}{\partial \theta_i} = \frac{m_i v_0^2}{6}(1-q)\sin 2\theta_i. \tag{26}$$

The precession frequency of the disc induced by the star cluster at different radii r is given by

$$\dot{\phi}_i = -\frac{v_0}{3r_i}(1-q)\cos\theta_i. \tag{27}$$

3.2 Numerical Setup

The numerical approach we use to study the time evolution of the disc is similar to the one presented in US09. There, we integrated the equations of motion for the rings after evaluating the steadily precessing equilibria for the given parameters to test the stability of those configurations. For the parameters relevant to the GC disc we do not find such steadily precessing equilibria. In an earlier work it is shown that centrally illuminated discs around black holes might under certain circumstances be warped by large angles, e.g. even by $\theta \sim \pi$ (Pringle 1997). The final geometry of the warped disc depends on the model assumptions like the strength of the perturbation leading to radiation instability and the location in the disc where the perturbation occurs. For the case of Bardeen-Petterson warping on the other hand, the degree of the warp depends on the initial mutual inclination between the angular momenta of the gaseous disc and the black hole. Therefore the most realistic initial disc shape for our simulations can only be chosen after carrying out simulations of gaseous discs subject to radiation instability, or Bardeen-Petterson effect, which is beyond the scope of this study. Therefore, without attempting to find such precise initial conditions, we adopt as initial warp shapes, the disc configurations which are likely to be imposed by the warping mechanisms discussed in the previous sections. Specifically, all the models are assigned an initial warp profile such that the inclinations range from -30° to 30°, and the azimuthal angles are zero. We note that this choice of the inclinations is in the range of the so-far reported values for either of the mechanisms. Fig. 3 depicts the initial inclination profile for the models we constructed.

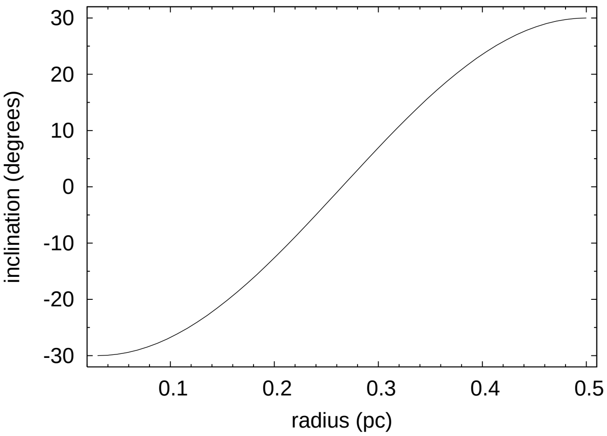

Figure 3. Initial inclination profile of the model discs.

In our simulations, we model a disc as a collection of 50 equally spaced, circular rings. The model discs extend between $0.03 - 0.5$ pc, surrounding a black hole of mass $M_{\rm bh} = 4 \times 10^6 M_\odot$. The surface density of the discs decline as $1/r^{1.4}$ as indicated by the observations. Initially, the discs are given a precession frequency such that when normalized to the orbital frequency of the innermost ring it gives $\dot{\phi}/\Omega_{\rm in} = -10^{-5}$. Below we will often give evolution times in terms of the orbital time at the inner edge of the disc, $({\rm P_{orb}})_{\rm in} \approx 244$ yr. We consider discs which are under the influence of only self-gravity (models SG), and discs which experience the effects of the star cluster and the self-gravity together (models CLSG). We assume three different mass fractions, $M_{\rm d}/M_{\rm bh}$ =0.00134, 0.0134, and 0.134 (LM-low mass, IM-intermediate mass, and HM-high mass respectively). We note that assuming $M_{\rm d}/M_{\rm bh} = 0.00134$ implies a star formation efficiency of $\epsilon_{\rm SF} = 1$, a value for which warping the planar GC disc is most plausible (see §2). However, in order to keep our discussion broad, and to make our models applicable to systems other than the GC, we also explore mass fractions which are higher than that inferred from the observations of the GC discs.

Observations of the nuclear star cluster of the GC suggest a mass range of $M_\star \sim [1-2] \times 10^6 M_\odot$ within the outer edge of the discs at 0.5 pc (Trippe et al. 2008; Schödel et al. 2009). Therefore, for the CLSG models, we set the quantity $v_0^2(1-q)$ that determines the strength of the cluster torque to 860 km^2 s^{-2} (see equation (26)). This value can be obtained, for example by setting the cluster mass within 0.5 pc to $10^6 M_\odot$, hence adopting a circular velocity of $v_0 \sim 93$

Simulation	$M_{\rm d}/M_{\rm bh}$	$r_{\rm in} - r_{\rm out}$ (pc)	$\Delta\theta$ (degrees)	$\lvert\dot{\phi}/\Omega_{\rm in}\rvert$	$v_0^2(1-q)$ (km^2 s^{-2})	$\tau_{\rm p}$ (10^6 yr)	Disc Break Up
SG_HM	0.13400	0.03-0.5	60	10^{-5}	-	0.6	yes
SG_IM	0.01340	0.03-0.5	60	10^{-5}	-	8	yes
SG_LM	0.00134	0.03-0.5	60	10^{-5}	-	60	no
CLSG_HM	0.13400	0.03-0.5	60	10^{-5}	860	0.35	yes
CLSG_IM	0.01340	0.03-0.5	60	10^{-5}	860	0.8	yes
CLSG_LM	0.00134	0.03-0.5	60	10^{-5}	860	1.6	no

Table 1. Parameters of the simulations discussed in the paper. The first column shows the label of the simulation. SG models are those considering only the self-gravity of the disc, while CLSG models include the effects of the star cluster as well. HM, IM, and LM stand for high mass, intermediate mass, and low mass respectively, which refer to the mass fractions given in column two. The third, the fourth, and the fifth columns show the adopted radial range, the overall warp, and the normalized initial precession frequency respectively. The sixth column gives the value of the quantity $v_0^2(1-q)$ which measures the strength of the torque from the star cluster. The seventh column lists the precession times attained at the end of each simulation, where the last column summarizes the behavior of the disc in terms of its coherence. The underlined parameter values follow from the observations or the models, whereas the others are assumed values.

km/s as induced by the star cluster, and the flattening of the cluster to $q = 0.9$.

The parameters of the simulations along with the resulting precession time scales and evolution are listed in Table 1. In these simulations, the total energy of the rings is typically conserved to an accuracy of 10^{-5}.

4 RESULTS

In this Section, we describe the main results that emerged from our simulations. We discuss in turn the precession of the model discs and the evolution of the discs' warp shapes.

4.1 Precession of the Disc

The self-gravity and the star cluster torques will force the disc to precess on time-scales proportional to the disc mass fraction, and the quantity $v_0^2(1-q)$ respectively (see equation (28) in US09 for the case of purely self-gravitating discs). The overall evolution of the disc will then be determined by the relative strengths of both torques.

In Fig. 4 we show for the SG models how the precession frequencies evolve during the simulations. The x-axis shows the elapsed time in terms of the orbital frequency of the innermost ring on the lower x-axis, and in units of 10^6 yr on the upper x-axis. The y-axis shows the absolute value of the averaged precession frequency, i.e. $|\sum_{i=1}^{n} \dot{\phi}_i/n|$. The red (upper), the black (middle) and the blue (lower) curves correspond to disc mass fractions of $M_{\rm d}/M_{\rm bh} = 0.13400$, $M_{\rm d}/M_{\rm bh} = 0.01340$, and $M_{\rm d}/M_{\rm bh} = 0.00134$ respectively. We see that although the average precession frequencies exhibit small oscillations in amplitude, they attain their true values (imposed by the disc's gravity) soon after the simulation starts, remaining approximately constant even though the shape of the disc evolves, as is shown in the next subsection. While individual rings may precess in the forward direction for short time intervals, most rings precess backwards for most of the time, so that the average precession is always retrograde.

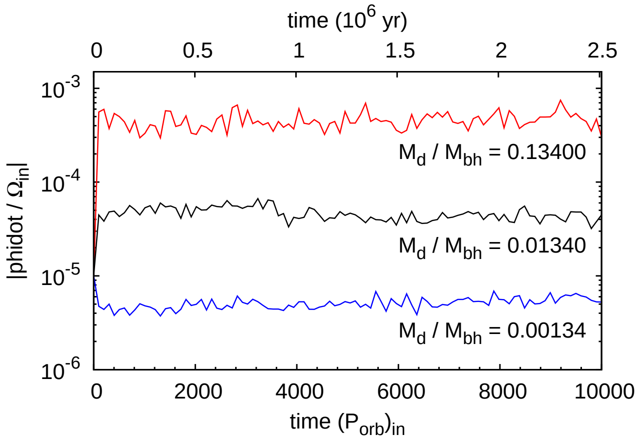

Figure 4. Evolution of the precession frequencies of the models considering only self-gravity of the disc. Different curves correspond to models with different mass fractions. The precession frequency increases in proportion to the disc mass fraction.

Throughout the simulation model SG_HM precesses with a normalized frequency of about -4×10^{-4}, corresponding to a precession time scale of $\tau_{\rm p} \approx 6 \times 10^5$ yr. For model SG_IM the normalized precession frequency drops to approximately -3×10^{-5} giving $\tau_{\rm p} \approx 8\times10^6$ yr, and when the mass fraction is decreased even further we see from model SG_LM that $\dot{\phi}/\Omega_{\rm in} = -4 \times 10^{-6}$ leading to $\tau_{\rm p} \approx 6 \times 10^7$ yr. (In order to check this, we have computed for model SG_LM the normalized precession frequencies that the rings would have under the self-gravity torques when the initial warp profile is considered (see equation (14) in US09). The values are in the range $[-8, -2] \times 10^{-6}$, with some of the rings having $\dot{\phi}/\Omega_{\rm in} \sim -4 \times 10^{-6}$, consistent with Fig. 4.) We can readily conclude from this, that the precession frequencies scale with disc mass. In the equations of motion, when the quadratic term for the precession frequency is set to zero, all terms scale linearly with ring mass so the precession frequency should indeed be proportional to the mass. Among the models discussed above only SG_HM would have completed a full precession during the life time of the stars.

In Fig. 5 we display how the above scaling manifests itself when we look at the averaged azimuthal angles of the

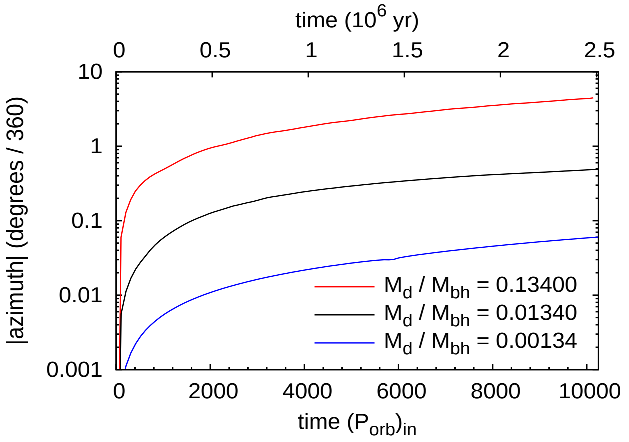

Figure 5. Precession of the models considering only self-gravity of the disc. Different curves correspond to the models with different mass fractions: the red (upper) curve is for model SG_HM, the black (middle) curve is for model SG_IM, and the blue (lower) curve is for model SG_LM. The ever faster precession of the more massive discs can be clearly seen.

rings, where the averaging is done in a similar way as for the frequencies. The different curves correspond to the different mass fractions again. At the end of the simulation, 10000 orbital periods after the simulation has started, model SG_HM is seen to have precessed approximately 4.5 times, while model SG_IM has completed nearly half a precession. The precession of the least massive model SG_LM on the other hand can barely be noticed with 0.05 times a full precession.

We now move on to the models including the effect of a surrounding cluster. In Fig. 6 we show the evolution of the averaged precession frequencies for the CLSG models. In contrast to the SG models, the precession frequencies for the CLSG models may not reach a constant value (note that the noise in the curves is the same as in Fig. 4, given the axis scaling). Until 3000 orbital periods, the frequencies of all the models increase linearly in time. Since the parameters of the star cluster are the same for all the models, it is again the most massive disc which precesses with the highest rate $\dot{\phi}/\Omega_{\rm in} = -7 \times 10^{-4}$ corresponding to a precession time scale $\tau_p \approx 3.5 \times 10^5$ yr. Comparing models SG_HM and CLSG_HM, we see that the averaged precession rates are approximately the same for the first 1000 orbital periods. At the end of the simulations, the star cluster leads to an approximately 2 times faster precession than in the self-gravitating case when $M_{\rm d}/M_{\rm bh} = 0.134$. For model CLSG_IM the precession is slower due to the decreased disc mass, but attains a value of $\dot{\phi}/\Omega_{\rm in} = -3 \times 10^{-4}$ giving $\tau_p \approx 8 \times 10^5$ yr, 10 times shorter than for model SG_IM due to the influence of the star cluster. Finally the lowest mass disc model including the star cluster CLSG_LM has $\dot{\phi}/\Omega_{\rm in} = -1.5 \times 10^{-4}$ and $\tau_p \approx 1.6 \times 10^6$ yr, which is nearly 40 times shorter than for SG_LM.

It emerges from these comparisons that the effect of the star cluster on the disc is most pronounced when the disc mass is low, otherwise the self-gravity torques dominate the evolution of the disc. In Fig. 7 we show for different mass fractions the expected ratio (based on equation (26) and equations (13) in US09) of the cluster torque, $\rm T_{cl}$, to the self-gravity torque, $\rm T_{cl}$, at different locations in the disc when the initial warp profile is considered. One can see that the low mass disc is indeed dominated by the cluster, while the high mass disc is dominated by self-gravity except in the inner parts. The kink and drop around ~ 0.25 pc is caused by the change of sign of the torques which follows from the choice of the warp profile.

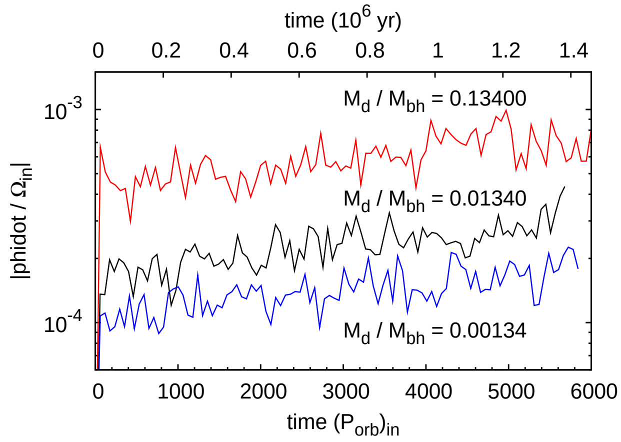

Figure 6. Evolution of the precession frequencies of the models including the torques from self-gravity and from the surrounding star cluster. Different curves correspond to models with different mass fractions as indicated on the labels.

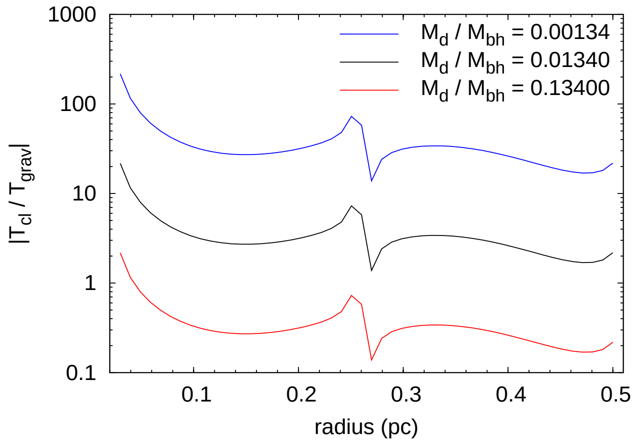

Figure 7. The comparison of the cluster torques, $\rm T_{cl}$, to the self-gravity torques $\rm T_{grav}$ acting on the rings. The low mass disc is dominated by the torques from the star cluster, while the high mass disc is dominated by self-gravity torques.

The relative effects of the cluster and the self-gravity torques can also be observed in the azimuthal profiles, i.e. radius versus azimuth, of the CLSG models which we show in Fig. 8. The black horizontal dotted line shows the initial profile of the azimuthal angles. The red curve with filled circles shows the azimuthal profile of model CLSG_HM towards the end of the simulation. The black curve with filled triangles, and the blue curve with filled squares depict the profiles of models CLSG_IM, and CLSG_LM respectively.

In general, it is possible to find disc configurations where the azimuthal angles of the rings are aligned even in the pres-

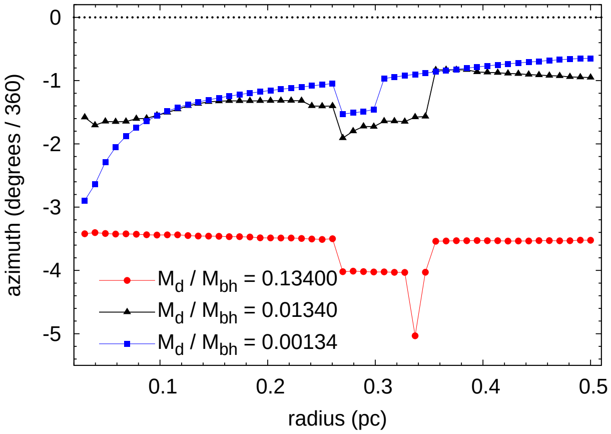

Figure 8. Azimuthal profiles of the CLSG models showing precession angles for all rings after 6000 inner periods. The black horizontal dotted line at the top shows the initial configuration. The red curve with filled circles shows the azimuthal profile of model CLSG_HM. The black curve with filled triangles, and the blue curve with filled squares depict the profiles of models CLSG_IM, and CLSG_LM respectively. The effect of the star cluster on the disc is best observed for model CLSG_LM where the azimuthal angles exhibit a differential profile.

ence of a surrounding star cluster (US09), however this can only be achieved for certain combinations of the disc parameters. Although for the GC parameters such configurations were not found, we see from Fig. 8 that an almost steady precession can be achieved when the disc is massive enough as in model CLSG_HM. In this case, the inner and the outer parts of the disc are locked together, while the middle parts which are ahead of the others are also seen to precess together. For model CLSG_IM where the effect of the self-gravity torques is diminished, the star cluster torques start to dominate in the inner parts of the disc, where the azimuthal profiles show more of a differential profile rather than a flat one. Since the rate of precession induced by the star cluster decreases going outwards in the disc (see equation (27)), the outer parts for this mass fraction are still held by the self-gravity of the disc. For the lowest mass model CLSG_LM, we see that the star cluster torques dominate over the self-gravity torques and the rings making up the disc can not precess with a common azimuth.

4.2 Evolution of the Inclinations and Breaking Up of the Disc

In this section we will discuss how the initial warp shape of the disc is modified under the self-gravity and the star cluster torques. Again, if we had started the simulations adopting equilibrium inclinations, we could expect to see that for a range of parameters, the discs would be stable, hence would not change their inclinations. Since we have seen in the previous section that even in the absence of an equilibrium configuration, some discs can maintain a near steady precession -at least at the inner and outer parts of the disc-, we might expect to see some behavior mimicking equilibrium in the the long term evolution of the inclinations as well.

In the plots we will be depicting in this section, the x-axis will show the elapsed time in terms of the orbital period of the innermost ring on the lower x-axis, and in units of 10^6 yr on the upper x-axis. The y-axis will show the ring inclinations, where the negative ones correspond to the inner parts, and the positive ones correspond to the outer parts. At any instant of time t, a vertical cut through the plot will then give the warp profile, i.e. the inclination at all radii.

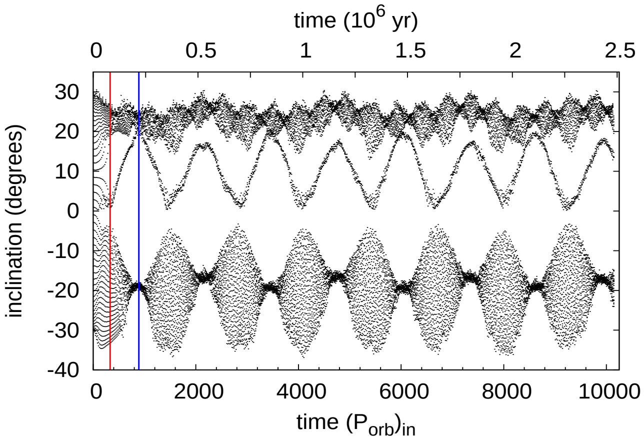

Figure 9. Time evolution of the inclinations for model SG_HM. The disc breaks into separate pieces which become pronounced after 330 orbital periods (marked by the vertical red (left) line). After 890 orbital periods (marked by the vertical blue (right) line) the inclinations reach a maximum separation of about 40°.

We start our discussion by considering first the SG models. In Fig. 9 we show the evolution of the individual ring inclinations for model SG_HM. We see that soon after the simulation starts the disc breaks into pieces, where the rings lying in the middle parts are pushed to more polar orbits, and the edge rings become more equatorial. After 330 orbital periods (indicated by the red (left) vertical line), the breaking of the disc becomes very prominent, leading to a configuration of three concentric, separate discs, the middle one being the less warped one. At about 890 orbital periods (indicated by the blue (right) vertical line), the two positively inclined discs merge together, and the separation between the inner and the outer discs reaches a maximum of about 40°. At this phase, the inner disc becomes almost planar, while the outer one is warped by about 10°. At about 1480 orbital periods the inclinations of the inner rings approach their initial values, and the mutual inclination of the separated discs become $\sim 25°$. After this time, subsequent oscillations with almost equal amplitude and period follow. Although a more detailed investigation of this behavior is beyond the scope of this study, we should note that these oscillations are reminiscent of stable oscillations for which the system parameters oscillate around their equilibrium points once perturbed.

In Fig. 10 we show the warp evolution of model SG_IM. We see again that the disc breaks into pieces. For this model however the breaking becomes pronounced at about 3300 orbital periods (indicated by the red (left) vertical line), 10 times longer than for model CLSG_HM corresponding to the 10 times longer precession time. At this stage, the disc has broken into three pieces, with similar characteristics, i.e. the

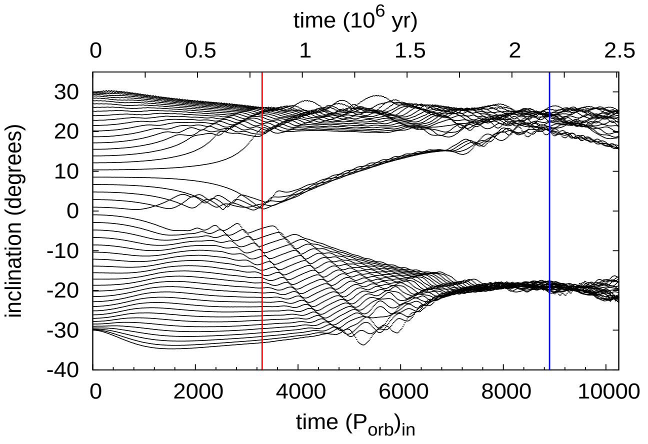

Figure 10. Time evolution of the inclinations for model SG_IM. The evolution is very similar, but retarded by a factor of 10, with respect to the evolution of model SG_HM.

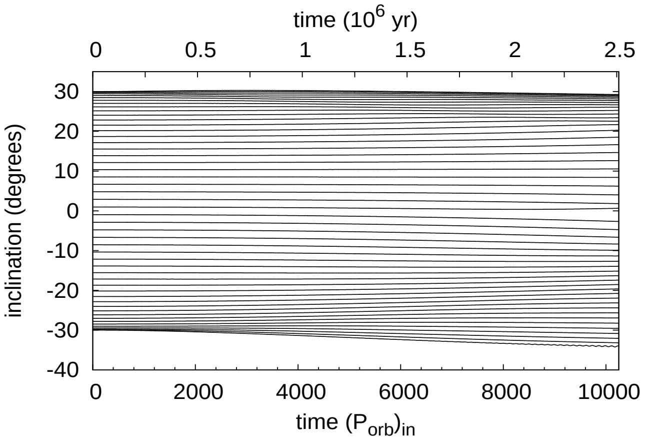

Figure 11. Time evolution of the inclinations for model SG_LM. The inclinations stay almost unaltered during the simulation which is an effect of the low mass fraction adopted.

degree of the warps, and the separation between the other discs, to those in model CLSG_HM. At about 8900 orbital periods (indicated by the blue (right) vertical line), the two of the positively inclined discs combine to form a single one, which is again separated by 40° from the negatively inclined one.

The warp evolution of model SG_LM is shown in Fig. 11. The inclinations of the rings for this model are seen to remain almost unchanged during the simulation. This is an effect of the low mass adopted for this model, and the corresponding long precession time. In order for this model to show a prominent breaking, the disc would have to evolve for about 3.3×10^4 orbital periods ($\approx 8 \times 10^6$ yr), which is longer than the age of the stars.

In Fig. 12 we show the warp evolution of model CLSG_HM which considers the effect of both the self-gravity and the star cluster. We have seen in the previous subsection that for this mass fraction, it is the self-gravity that mainly dominates the precession evolution of the disc. The situation is therefore similar to that in Fig. 9 when we consider the warp evolution. We see that model CLSG_HM also breaks into pieces on time scales comparable to those for model SG_HM, attaining similar separation angles. More specifically, model CLSG_HM reaches a maximum separation of 40° at about 600 orbital periods. At 1300 orbital periods, the mutual inclination between the broken parts drops to 10°. This is twice the value attained in model SG_HM. However, the major difference between the two models shows itself in the long term evolution, the cluster model exhibiting a less well behaved oscillation pattern.

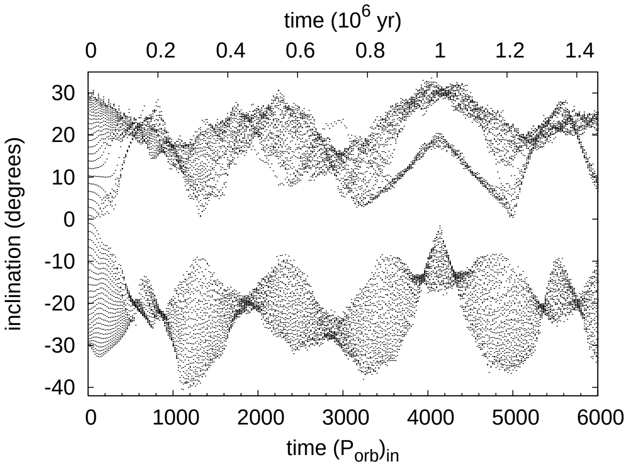

Figure 12. Time evolution of the inclinations for model CLSG_HM. The disc breaks into pieces on time scales comparable to those for model SG_HM. The long time behavior of these two models differ in that when the cluster is present, the oscillations in inclination are less well behaved.

When the mass fraction is decreased, the effect of the cluster torques become more prominent. This can be seen in Fig. 13. After about 500 orbital periods the ring inclinations start to deviate from their original values.

Compared to the other models in which the disc breaks up, the evolution for this model is more disordered. There is no well defined pattern left in the warp profile once the disc breaks. After 2500 orbital periods, the positively inclined rings are pushed to inclinations of more than 30°, reaching a maximum of about 50° at the end of the simulation. At this stage, only some of the inner rings exhibit a disc-like structure with a warp of about 10°. The original disc as a whole has dissolved due to the differential precession induced by the cluster, and the self-gravity of the disc is not able to hold the disc intact.

In Fig. 14 we show the evolution of inclinations for model CLSG_LM. For this model, we see that the inclinations are altered by only a few degrees, which at the end of the simulation leave the overall warp shape almost unchanged. This is because for this model the torques are dominated by the star cluster, leading to nearly free differential precession of the rings at constant inclination, causing the rings to spread in azimuth by about one full rotation (see Fig. 8).

In the last part of this section, we show in Fig. 15 several examples of the 3-dimensional visualizations of our models at different stages of their evolution. The color code displays the height (z-coordinate) of the disc. Different viewing angles are chosen to highlight the various structures present in the warp shapes. The figures correspond to: the initial con-

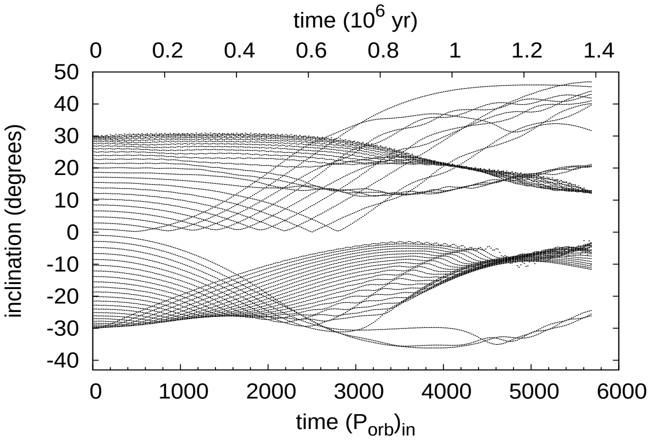

Figure 13. Time evolution of the inclinations for model CLSG_IM. The self-gravity of the disc can not hold the rings together, and the disc breaks up into several fragments under the influence of the star cluster.

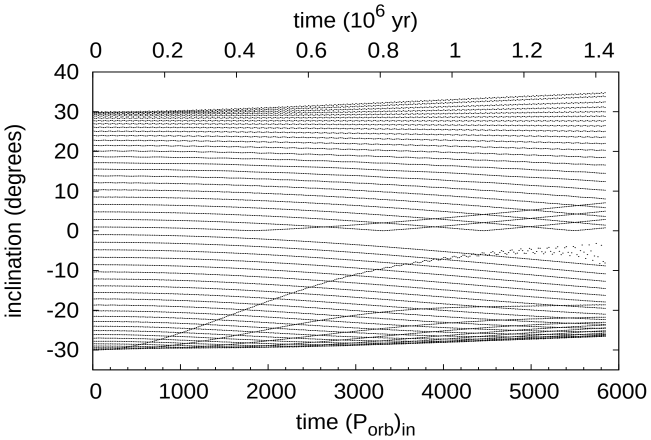

Figure 14. Time evolution of the inclinations for model CLSG_LM. The inclinations do not change substantially while the rings precess apart azimuthally (see Fig. 8), because the mass fraction adopted is low for this model.

figuration common to all the models (a), model SG_HM at $\hat{t} = 340$ (b), model SG_IM at $\hat{t} = 8900$ (c), model CLSG_IM at $\hat{t} = 2500$ (d), model CLSG_IM at $\hat{t} = 5680$ (e), and model CLSG_LM at $\hat{t} = 5680$ (f) respectively where $\hat{t} = t/P_{\mathrm{orb}_{\mathrm{in}}}$. The broken shapes of the discs after some evolution for models SG_HM and SG_IM are apparent in figures (15b) and (15c). Fig. (15e) depicts clearly how the shape of a disrupted disc with parameters identical to those for model CLSG_IM would look like. In the last panel in Fig. (15f), we see that the inner parts of the disc precessed more compared to the outer parts, while the inclination of the disc has only slightly changed compared to its initial state (see figures (8) and (14)).

4.3 Comparison With the Observations

In this section, we compare our time evolution models with the observations of the GC discs. In doing so, we will make use of the results of Bartko et al. (2009, 2010).

After application of proper selection criteria, the sample includes a total of 136 stars on clockwise and counter-clockwise rotating orbits. These stars have measured (x, y) position, while the line-of-sight distance z is unknown. For the analysis, z is therefore treated with a Monte-Carlo simulation. The respective space velocities v_x, v_y, and v_z are also given in Bartko et al. (2009).

The number density of stars in the discs, $\Sigma_{\mathrm{nr}}(r)$, scales as $1/r^{1.4}$ (Bartko et al. 2010). Here r is the 3-dimensional distance to SgrA*, corresponding to the radius r of our rings. The total number of stars on a ring is then $2\pi r \Delta r \Sigma_{\mathrm{nr}}(r)$. If we assume that the total number of stars in the disc is N_{t} we can write

$$\sum_{1}^{n} 2\pi r \Delta r \Sigma_{\mathrm{nr}}(r) = N_{\mathrm{t}}, \tag{28}$$

where n is the number of rings making up the disc. We write $\Sigma_{\mathrm{nr}}(r) = \Sigma_0 (r/r_{\mathrm{in}})^{-1.4}$. The normalization Σ_0, i.e the number of stars on the innermost ring, is then obtained by writing

$$\Sigma_0 = \frac{N_t}{2\pi \Delta r \; r_{\mathrm{in}}^{1.4} \displaystyle\sum_{1}^{n} \frac{1}{r^{0.4}}}. \tag{29}$$

The coordinates of a star on a ring are given by

$$\begin{aligned} x &= r(\cos\phi\cos\psi - \cos\theta\sin\phi\sin\psi), \\ y &= r(\sin\phi\cos\psi + \cos\theta\cos\phi\sin\psi), \\ z &= r\sin\theta\sin\psi. \end{aligned} \tag{30}$$

In order to construct the phase space distributions of the stars populating the discs, we write the components of the stellar velocities

$$\begin{aligned} v_x &= r(\dot\theta\sin\theta\sin\psi\sin\phi - \dot\psi\sin\psi\cos\phi - \dot\phi\sin\phi\cos\psi \\ &- \dot\phi\cos\theta\cos\phi\sin\psi - \dot\psi\cos\theta\sin\phi\cos\psi), \\ v_y &= r(\dot\phi\cos\phi\cos\psi - \dot\phi\cos\theta\sin\phi\sin\psi \\ &+ \dot\psi\cos\theta\cos\phi\cos\psi - \dot\theta\sin\theta\sin\psi\cos\phi - \dot\psi\sin\psi\sin\phi), \\ v_z &= r(\dot\theta\sin\psi\cos\theta + \dot\psi\sin\theta\cos\psi). \end{aligned} \tag{31}$$

Since we know the values of $(\dot\phi, \dot\theta, \dot\psi, \phi, \theta)$ from our time integration, we can generate a random sample of stars on these rings, by dicing ψ. We can then construct the phase space distribution of stars at each instant of time t using equations (30) and (31) .

The GC contains two warped and almost orthogonal discs of young stars which extend over a similar range of projected radii (Bartko et al. 2010). The CW disc is observed to extend between projected radii of approximately 0."8 and 15", while the CCW disc is seen between projected radii of about 3."5 and 15". This makes it unlikely that the two stellar discs derive from a single progenitor disc, but rather suggests that they might be tracers of two separate accretion episodes. In the following, we will concentrate in our model comparison on the CW disc, which is better defined due to its larger number of constituent stars.

We have shown in the previous section that massive discs break into pieces. Although the broken discs may precess as coherent separate discs under certain circumstances, their degree of warping is highly reduced compared to the original disc. The observational analysis presented in

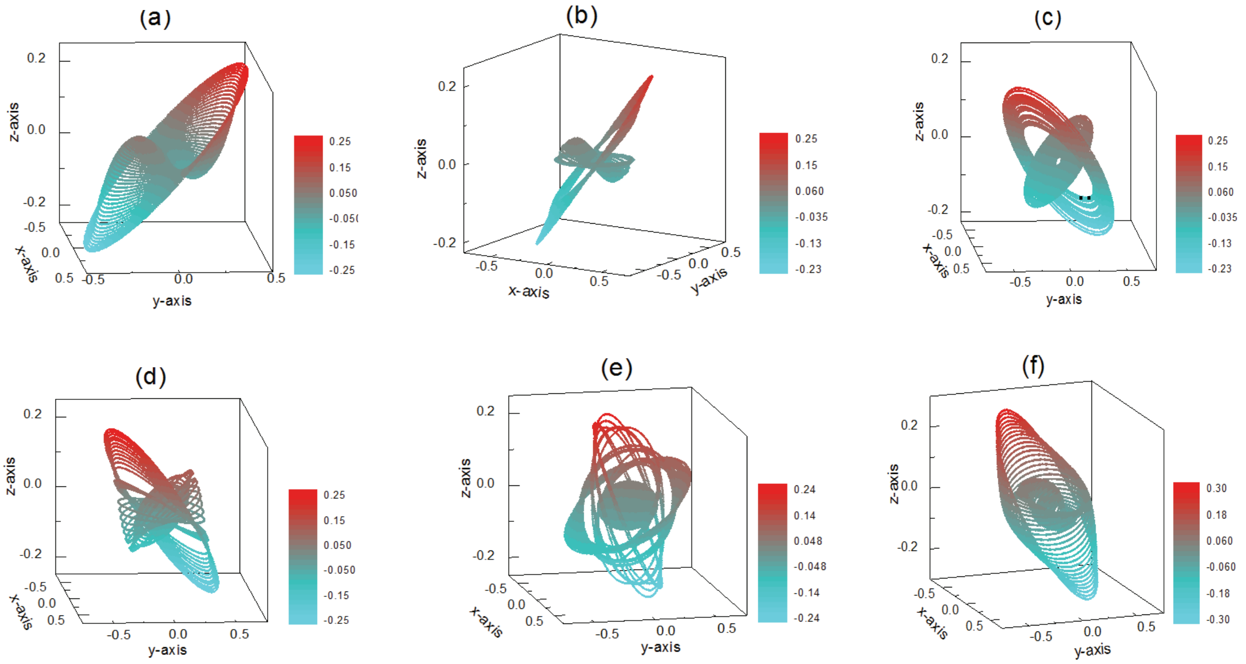

Figure 15. 3-dimensional visualizations of the warped disc models at different stages of their evolution. The color code displays the height (z-coordinate) of the disc. Different viewing angles are chosen to highlight the various structures present in the warp shapes. The figures correspond to: the initial configuration common to all the models (a), model SG_HM at $\hat{t} = 340$ (b), model SG_IM at $\hat{t} = 8900$ (c), model CLSG_IM at $\hat{t} = 2500$ (d), model CLSG_IM at $\hat{t} = 5680$ (e), and model CLSG_LM at $\hat{t} = 5680$ (f) respectively where $\hat{t} = t/P_{\mathrm{orb_{in}}}$.

Bartko et al. (2009) can discriminate between a disc precessing as a single unit and a broken disc, such that the former produces a warp profile that changes gradually between the inner and the outer radii, while the latter would result in a jump at a certain radius.

A useful way of comparing the models with the observations is to construct the components of angular momenta and see how they change with projected radius. The component of angular momentum along the axis pointing towards the observer will then give information on the twist of the disc, while the component projected onto the plane of the sky will give the degree of the warp (for further details on the definitions of the angles see Bartko et al. (2009)).

Fig. 16 shows the component of the local average angular momentum direction of the model discs (red triangles), and of the CW disc as published in Bartko et al. (2009) (blue dots) on the plane of the sky as a function of average projected distance from the centre (l=$\phi_J(R)$ in the notation of Bartko et al. (2009) where J denotes the angular momentum per mass). The data from the simulations is rotated successively such that the orientations of the model and the observed discs match at the inner edge, and the warp in the simulations fit the observed warp best. The points referring to the simulations are chosen at certain times during the late stages of the evolution of the discs. The figures on the top are for the self-gravity-only models, and the ones at the bottom are for the models including the effects of the star cluster. The mass fraction of the simulated discs decreases going from left to right, therefore the models should be read as HM, IM, and LM going in this direction.

We see that a good agreement with the observations of the CW disc is achieved for our model SG_LM in that the inclination (warping of the disc) changes gradually between the inner and the outer edges of the disc, and that the amplitude of the warp is successfully reproduced. For the self-gravity-only models, higher mass fractions lead to flattening of the inner parts of the disc, hence can be excluded to be representative of the data. On the other hand, when the torques from the star cluster are taken into account, none of these models seem to match the data well.

5 DISCUSSION

5.1 Dependence on the Initial Conditions

In the previous section we argued that a good agreement with the observations of the CW disc is achieved for our model SG_LM. To test the importance of the choice of the initial warp configuration we performed a run, model LI, where the initial inclinations, i.e. $\Delta\theta$, span a range -15° to 15°, and the other set of parameters are identical to those of model SG_LM. Fig. 17 shows the evolution of the azimuthal angles for models LI (solid line), and SG_LM (dashed line). We see that when the disc is less inclined it precesses faster, by a factor of about 1.3 for the parameters chosen. An analytic expression showing the inverse proportionality of the precession rate to the disc inclination for steadily precessing discs can be found in US09.

We show in Fig. 18 the evolution of the ring inclinations for model LI. We see that the splitting of the disc into parts, although not much pronounced, occurs on a shorter time

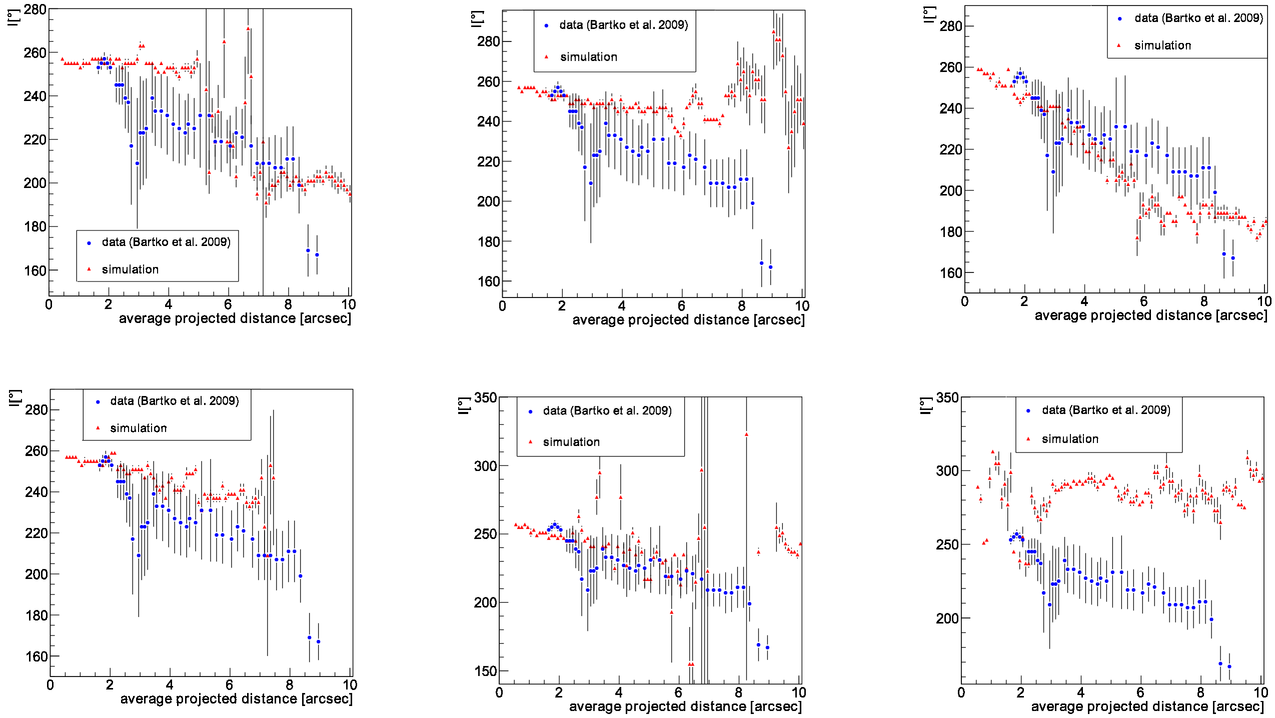

Figure 16. The warp profiles of the model discs (red triangles) and of the CW disc (blue dots). The figures on the top show the self-gravity-only models, and the ones at the bottom show the models including the effects of the star cluster. The mass fraction of the simulated discs decreases going from left to right. The lowest mass model for the case of self-gravity-only gives the best agreement with the data.

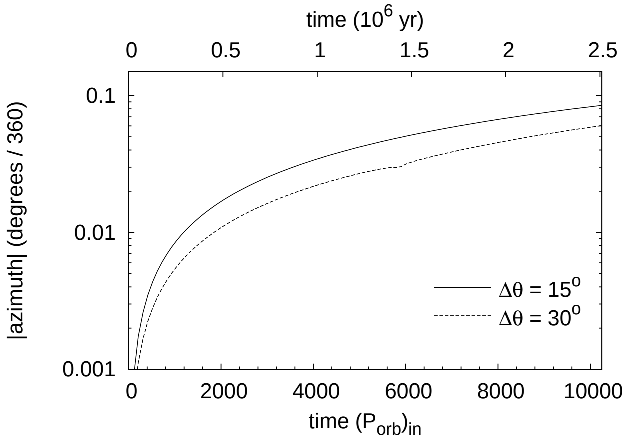

Figure 17. Time evolution of the azimuthal angles for models LI (solid line), and SG_LM (dashed line). Model LI precesses 1.3 times faster than model SG_LM due to its decreased overall inclination.

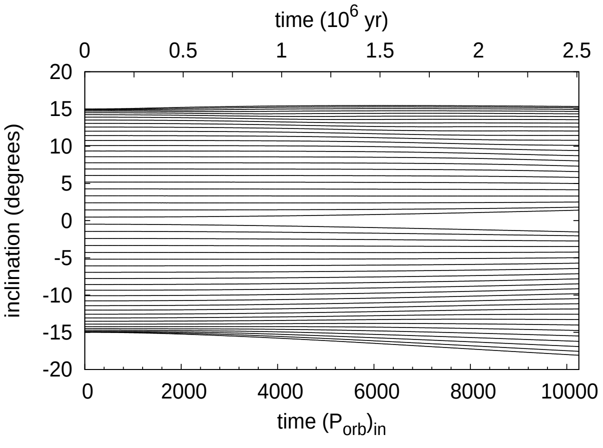

Figure 18. Time evolution of the ring inclinations for model LI. The ring inclinations change only slightly throughout the simulation, leading to a final warp of about 32°.

as compared to model SG_LM (the inclinations in model SG_LM had remained unaltered during a similar time span). Even if there are slight excursions of the ring inclinations from their initial values, the overall warp shape does not change considerably throughout the simulation for model LI either. Hence we conclude that in order for the low mass disc to evolve towards the observed orbital configuration, its initial inclination determined by the warping mechanisms has to be close to the observed inclination.

5.2 Comparison to Linear Evolution

In US09 it is shown that linear theory over estimates the torques acting on the edges of the disc, leading to a slightly less inclined warp configuration at its maximum possible value (within the validity of the linear theory). Here, we would like to briefly discuss the evolution of the disc in linear theory, where the linearization is done as in US09. In order to reduce computational time we have considered one purely self-gravitating model adopting a mass fraction of

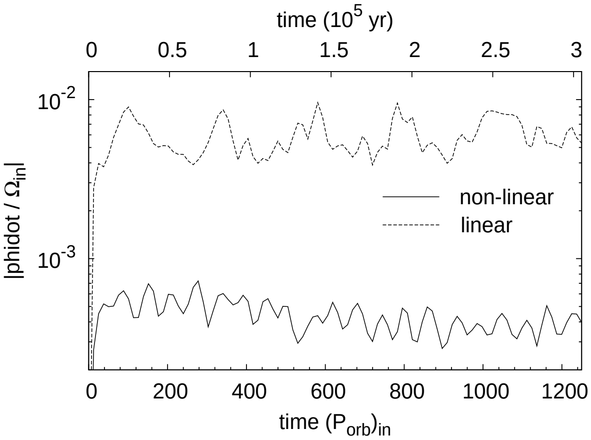

Figure 19. Average precession frequencies attained during the simulations for a mass fraction of $M_\mathrm{d}/M_\mathrm{bh} = 0.134$. The solid line is for model SG_HM calculated in the non-linear torques regime, and the dashed line is for the linear model. The disc precesses with a much higher rate in the linear regime.

$M_\mathrm{d}/M_\mathrm{bh} = 0.134$. We have run the simulation for about $1250\mathrm{P}_{\mathrm{orb}_\mathrm{in}}$, which corresponds to half a precession time for the non-linear model for this mass fraction. Since the evolution of the disc scales approximately linearly in mass, the comparison which we will present should equally apply to discs with other mass fractions.

In Fig. 19 we show the averaged precession frequencies of the non-linear (model SG_HM) (solid line), and the linear models (dashed line). We see that in linear theory the model acquires an average precession frequency of $\dot{\phi}/\Omega_\mathrm{in} \approx -6 \times 10^{-3}$, corresponding to a precession time scale of 4×10^4 yr. Hence the model disc in linear theory precesses 15 times faster than it should. Turned around, the system behaves as if it were 15 times more massive (for the mass fraction considered here, this would unphysically indicate a disc twice more massive than the central black hole).

5.3 Limitations

5.3.1 Eccentricity of the Disc

In our simulations, we used a simple circular ring model although the observations point to an eccentricity of the orbits with $e \sim 0.35$ for the CW disc and close to zero eccentricity for the CCW disc (Paumard et al. 2006; Bartko et al. 2009, 2010). The change of eccentricity (as well as inclination) in an initially circular disc might be driven by the interaction of the disc stars with the surrounding cusp (Perets et al. 2008; Löckmann et al. 2009). Following the time evolution of single and initially mutually inclined two discs, Löckmann & Baumgardt (2009) showed that such interactions can cause the inner parts of the disc, i.e. $r < 0.3$ pc, to gain quite high eccentricities on a typical time scale of 5 Myr. Neglecting the effects of the disc's self-gravity Madigan et al. (2009) showed that an initially eccentric disc embedded in a stellar cusp around a massive black hole is subject to an instability which leads to the growth of eccentricities on about a precession time (∼ 0.6-0.7 Myr at 0.05 pc). It is not known whether taking into account the self-gravity of the disc would modify the results of these calculations strongly.

5.3.2 Viscous Evolution of The Disc

In proposing our scenario, we made a strong assumption that there had been an accretion disc around SgrA* a few million years ago. While we have argued for the plausibility of disc warping prior to star formation, our simulations were performed following only the gravitational evolution of the disc. The next step forward would be to consider the viscous evolution of the disc under the non-linear self-gravity torques, as well as the torques from the old star cluster. As we will briefly discuss in the next subsection, viscous discs in various physical environments are also prone to be broken or disrupted by differential precession.

5.4 Vector Resonant Relaxation as a Warping Mechanism

In our scenario, we considered two mechanisms, the radiation instability, and the Bardeen-Petterson effect to explain the warped gaseous disc origin of the GC discs. Without making a detailed numerical analysis of these mechanisms, we argued for their possibility based on simple arguments such as the critical radii and time scales for warping. It would be interesting to explore other warping mechanisms than the two discussed here. Recently, Bregman & Alexander (2009) showed that vector resonant relaxation (VRR) resulting from the interaction of the disc with the surrounding old star cluster might explain the warp in the maser disc of NGC4258. When scaled to the parameters of the GC region, VRR serves as a viable mechanism for orbits within the central ∼ 0.2 pc (Kocsis & Tremaine 2011). Beyond this radius, the VRR time scale exceeds the life time of the disc stars. However, it would still be interesting to see how the disc responds to the stellar cusp when the simulations are carried out in the non-linear regime.

5.5 Broken/Disrupted Warped Discs

We have shown examples of purely gravitating warped disc simulations where the discs with a certain mass fraction break into pieces. This is an effect of the faster precession of some parts of the disc, and can lead to a complete disruption of the disc if the broken parts can not be held together by internal torques.

Broken or disrupted discs have been reported before mainly in the context of viscous discs. Accretion discs warped by tidal effects in misaligned binaries can be disrupted due to differential precession when the disc aspect ratio $h = H/r \sim 0.01$, where H is the disc height (Larwood et al. 1996; Fragner & Nelson 2010). When the warp propagation through the disc is diffusive rather than wave-like, isothermal discs with small viscosity exhibit a steepening in their warp profiles where the disc breaks into two parts (Ogilvie 2006; Lodato & Price 2010).

6 SUMMARY AND CONCLUSIONS

We have proposed a new scenario for the formation of the warped stellar discs of young stars at the Galactic Centre (GC). In contrast to the work published so far, our study is based on the assumption that the star formation at the GC took place in an accretion disc but was delayed until the accretion disc around SgrA* was warped. To test the plausibility of this idea we addressed the issue of accretion disc warping considering two mechanisms, the Pringle (radiation) instability, and the Bardeen-Petterson effect. From simple arguments we showed that warping of the GC disc is plausible if the star formation efficiency is high, $\epsilon_{\rm SF} \lesssim 1$, and the viscosity parameter $\alpha \sim 0.1$.

Our simulations are based on the idea that, some time after the disc became warped, the activity at the GC subsided. Rapid cooling of the disc led to fragmentation and star formation, while the rest of the gas was lost. Subsequently, the disk was subject only to gravitational forces causing it to precess. In addition to the torques from the self-gravity of the disc, the torques induced by a surrounding non-spherical star cluster were also taken into account in our models. We examined the long term temporal behavior of the warped disc models with different disc-to-black hole mass ratios (mass fractions), and investigated the interplay between the self-gravity and the cluster torques. We also made a comparison of our models with the observations of the warped GC discs. Our findings can be summarized as follows:

i) When the disc mass fraction is large, $M_{\rm d}/M_{\rm bh} \approx 0.1$, the disc breaks into distinct pieces which then precess independently. In this case, the self-gravity torques dominate over the torques from the star cluster, for cluster parameters representative for the GC. The warp profiles of these models evolve in an oscillatory manner which is very well behaved for the self-gravity model. The maximum mutual inclinations attained (about 40°), and the time scales by which the disc acquires this broken configuration are comparable in both models, despite a slightly faster precession of the cluster model.

ii) Moderate mass discs with $M_{\rm d}/M_{\rm bh} \approx 0.01$ evolve in two distinct ways, depending on the absence or presence of the torques from the star cluster. In the former case, the evolution of the model mimics that of its higher mass counterpart. Both the precession and the break-up of the disc occur on time scales which are almost exactly 10 times longer than for the high mass model. The model including the effect of the star cluster for this mass fraction exhibits a more disordered evolution. The disc breaks into parts more slowly, but once it arrives in a broken configuration, its pieces cannot stay intact due to the decreased self-gravity, and the disc as a whole dissolves.

iii) Low mass discs for which $M_{\rm d}/M_{\rm bh} \approx 0.001$ precess on time scales of order a few 10^7 yr when the disc is subject only to its own self-gravity, while the presence of the star cluster fastens the precession of the disc by about a factor of fourty for the estimated quadrupole moment of the star cluster. The overall inclination of the disc is not grossly altered during the simulations for this mass fraction. When only the self-gravity of the disc is considered, the disc precesses as a single body throughout its evolution, while inclusion of the torques from the star cluster cause the rings to precess apart.

iv) None of our models lead to a configuration where parts of a broken disc would counter-rotate on the plane of the sky, i.e. give rise to two mutually counterrotating discs. A comparison of our models with the better-defined clockwise rotating disc shows that the lowest mass self-gravity only model matches the data best. In this case in order for the model to mimic the observed orbital configuration of the stellar disc, its initial inclination determined by the gas disc warping mechanism has to be close to the observed one. On the other hand when the star cluster torques are taken into account, the overall shape of the warp can not be reproduced. The disagreement of the model including the star cluster might mean either that the old star cluster at the Galactic Centre is almost spherical so that it exerts no torque on the discs, or that the mass of the cluster within the radius of the disc is less than the value assumed here based on the most recent observations. Future observations of the old star cluster will therefore help to better understand the behavior of the stellar discs.

ACKNOWLEDGMENTS

A.U.S would like to thank M. Arnaboldi for sharing ideas on warped discs in a general context, and R. Sunyaev for pointing to useful literature in the early stages of this study. She also acknowledges the support of staff at CfA, Harvard University where part of this work was completed. This work is partially supported by the Scientific Research Projects Coordination Unit of Istanbul University under project number UDP-16581.

REFERENCES

Alexander, R. D., Armitage, P. J., Cuadra, J., & Begelman, M. C. 2008, ApJ, 674, 927

Armitage, P. J. & Natarajan, P. 1999, ApJ, 525, 909

Bardeen, J. M. & Petterson, J. A. 1975, ApJ, 195, L65+

Bartko, H., Martins, F., Fritz, T. K., Genzel, R., Levin, Y., Perets, H. B., Paumard, T., Nayakshin, S., Gerhard, O., Alexander, T., Dodds-Eden, K., Eisenhauer, F., Gillessen, S., Mascetti, L., Ott, T., Perrin, G., Pfuhl, O., Reid, M. J., Rouan, D., Sternberg, A., & Trippe, S. 2009, ApJ, 697, 1741

Bartko, H., Martins, F., Trippe, S., Fritz, T. K., Genzel, R., Ott, T., Eisenhauer, F., Gillessen, S., Paumard, T., Alexander, T., Dodds-Eden, K., Gerhard, O., Levin, Y., Mascetti, L., Nayakshin, S., Perets, H. B., Perrin, G., Pfuhl, O., Reid, M. J., Rouan, D., Zilka, M., & Sternberg, A. 2010, ApJ, 708, 834

Bonnell, I. A. & Rice, W. K. M. 2008, Science, 321, 1060

Bregman, M. & Alexander, T. 2009, ApJ, 700, L192

Cuadra, J., Armitage, P. J., & Alexander, R. D. 2008, ArXiv e-prints, 804

Fragner, M. M. & Nelson, R. P. 2010, A&A, 511, A77+

Gammie, C. F. 2001, ApJ, 553, 174

Genzel, R., Pichon, C., Eckart, A., Gerhard, O. E., & Ott, T. 2000, MNRAS, 317, 348

Genzel, R., Schödel, R., Ott, T., Eisenhauer, F., Hofmann, R., Lehnert, M., Eckart, A., Alexander, T., Sternberg, A., Lenzen, R., Clénet, Y., Lacombe, F., Rouan, D., Renzini, A., & Tacconi-Garman, L. E. 2003, ApJ, 594, 812

Ghez, A. M., Salim, S., Hornstein, S. D., Tanner, A., Lu, J. R., Morris, M., Becklin, E. E., & Duchêne, G. 2005, ApJ, 620, 744

Gillessen, S., Eisenhauer, F., Trippe, S., Alexander, T., Genzel, R., Martins, F., & Ott, T. 2009, ApJ, 692, 1075

Goodman, J. 2003, MNRAS, 339, 937

Greenhill, L. J., Booth, R. S., Ellingsen, S. P., Herrnstein, J. R., Jauncey, D. L., McCulloch, P. M., Moran, J. M., Norris, R. P., Reynolds, J. E., & Tzioumis, A. K. 2003, ApJ, 590, 162

Greenhill, L. J. & Gwinn, C. R. 1997, Astrophysics and Space Science, 248, 261

Haas, J., Subr, L., & Kroupa, P. 2010, ArXiv e-prints

Herrnstein, J. R., Greenhill, L. J., & Moran, J. M. 1996, ApJ, 468, L17+

Hobbs, A. & Nayakshin, S. 2009, MNRAS, 394, 191

Kocsis, B. & Tremaine, S. 2011, MNRAS, 412, 187

Kolykhalov, P. I. & Syunyaev, R. A. 1980, Soviet Astronomy Letters, 6, 357

Krabbe, A., Genzel, R., Eckart, A., Najarro, F., Lutz, D., Cameron, M., Kroker, H., Tacconi-Garman, L. E., Thatte, N., Weitzel, L., Drapatz, S., Geballe, T., Sternberg, A., & Kudritzki, R. 1995, ApJ, 447, L95+

Kumar, S. & Pringle, J. E. 1985, MNRAS, 213, 435

Larwood, J. D., Nelson, R. P., Papaloizou, J. C. B., & Terquem, C. 1996, MNRAS, 282, 597

Lense, J. & Thirring, H. 1918, Physikalische Zeitschrift, 19, 156

Levin, Y. & Beloborodov, A. M. 2003, ApJ, 590, L33

Löckmann, U. & Baumgardt, H. 2009, MNRAS, 394, 1841

Löckmann, U., Baumgardt, H., & Kroupa, P. 2009, MNRAS, 398, 429

Lodato, G. & Price, D. J. 2010, MNRAS, 405, 1212

Lodato, G. & Pringle, J. E. 2006, MNRAS, 368, 1196

—. 2007, MNRAS, 381, 1287

Lu, J. R., Ghez, A. M., Hornstein, S. D., Morris, M., Matthews, K., Thompson, D. J., & Becklin, E. E. 2006, Journal of Physics Conference Series, 54, 279

Lu, J. R., Ghez, A. M., Hornstein, S. D., Morris, M. R., Becklin, E. E., & Matthews, K. 2009, ApJ, 690, 1463

Madigan, A.-M., Levin, Y., & Hopman, C. 2009, ApJ, 697, L44

Maloney, P. R., Begelman, M. C., & Pringle, J. E. 1996, ApJ, 472, 582

Mapelli, M., Hayfield, T., Mayer, L., & Wadsley, J. 2008, ArXiv e-prints, 805

Martin, R. G. 2008, MNRAS, 387, 830

Milosavljević, M. & Loeb, A. 2004, ApJ, 604, L45

Nayakshin, S., Dehnen, W., Cuadra, J., & Genzel, R. 2006, MNRAS, 366, 1410

Ogilvie, G. I. 1999, MNRAS, 304, 557

—. 2006, MNRAS, 365, 977

Ogilvie, G. I. & Dubus, G. 2001, MNRAS, 320, 485

Papaloizou, J. C. B. & Pringle, J. E. 1983, MNRAS, 202, 1181

Paumard, T., Genzel, R., Martins, F., Nayakshin, S., Beloborodov, A. M., Levin, Y., Trippe, S., Eisenhauer, F., Ott, T., Gillessen, S., Abuter, R., Cuadra, J., Alexander, T., & Sternberg, A. 2006, ApJ, 643, 1011

Perets, H. B., Gualandris, A., Merritt, D., & Alexander, T. 2008, Mem. Soc. Astron. Ital., 79, 1100

Petterson, J. A. 1977, ApJ, 216, 827

Pringle, J. E. 1996, MNRAS, 281, 357

—. 1997, MNRAS, 292, 136

Schandl, S. & Meyer, F. 1994, A&A, 289, 149

Scheuer, P. A. G. & Feiler, R. 1996, MNRAS, 282, 291

Schödel, R., Merritt, D., & Eckart, A. 2009, A&A, 502, 91

Shakura, N. I. & Sunyaev, R. A. 1973, A&A, 24, 337

Sparke, L. S. 1986, MNRAS, 219, 657

Torkelsson, U., Ogilvie, G. I., Brandenburg, A., Pringle, J. E., Nordlund, Å., & Stein, R. F. 2000, MNRAS, 318, 47

Trippe, S., Gillessen, S., Gerhard, O. E., Martins, F., Eisenhauer, F., Ott, T., Maness, H. L., Dodds-Eden, K., & Genzel, R. 2008, submitted to A&A

Ulubay-Siddiki, A., Gerhard, O., & Arnaboldi, M. 2009, MNRAS, 398, 535